Journal of Sound and Vibration (1995) **184**(3), 503–528

MODELLING OF A HYDRAULIC ENGINE MOUNT FOCUSING ON RESPONSE TO SINUSOIDAL AND COMPOSITE EXCITATIONS

J. E. Colgate, C.-T. Chang, Y.-C. Chiou, W. K. Liu and L. M. Keer

Department of Mechanical Engineering, *Northwestern University*, *Evanston*, *Illinois* 60208, *U.S.A.*

(*Received* 14 *June* 1993, *and in final form* 24 *June* 1994)

Frequency response characteristics of a hydraulic engine mount are investigated. The mount studied is highly non-linear due to an amplitude-limited floating piston (the "decoupler") which enables the response to large amplitude (typically road-induced) excitations to differ markedly from the response to small amplitude (typically engine-induced) excitations. The effect of the decoupler on frequency response as well as composite-input (sum of two sinusoids) response is considered.

New experimental data for a production mount and several specially prepared mounts are presented and discussed. Two linear models, one for large amplitude excitations and one for small amplitude excitations, are developed and shown to be effective over a 5–200 Hz frequency range. The latter model explains a moderately high frequency ($\sim$120 Hz) resonance which is often observed in the data, but which has not previously been described in physical terms.

A piecewise linear simulation and an equivalent linearization technique are used to explain the amplitude-dependence of frequency response, as well as the composite-input response. The applicability of equivalent linearization is justified by demonstrating that high order harmonics contribute very little to the transmitted force. Moreover, this technique is found to be computationally efficient and to provide insight into decoupler dynamics.

1. INTRODUCTION

Engine mounts serve two principal functions: vibration isolation and engine support. In the past decade, the automotive industry's shift to small, four cylinder engines and transversely mounted front-wheel-drive powertrains has made these two functions increasingly incompatible. For instance, the lower firing frequencies of four cylinder engines coupled with lower engine inertia tend to excite higher amplitude vibrations. To avoid significant chassis vibration and passenger compartment noise, softer mounts become necessary—it is not uncommon for the elastic rate (stiffness) of a mount in a front-wheel-drive automobile to be 20 times less than that of a rear-wheel-drive automobile [1]. Engine mounts, however, must also limit or "control" engine excursions caused by rough roads, idle shake, vehicle accelerations and wheel torque reaction (which is especially an issue in front-wheel-drive). To provide control, it is important that the engine mounts be stiff and heavily damped. This growing disparity between isolation characteristics and control characteristics has profoundly changed the way in which the industry approaches mount design.

0022–460X/95/280503 + 26 $12.00/0

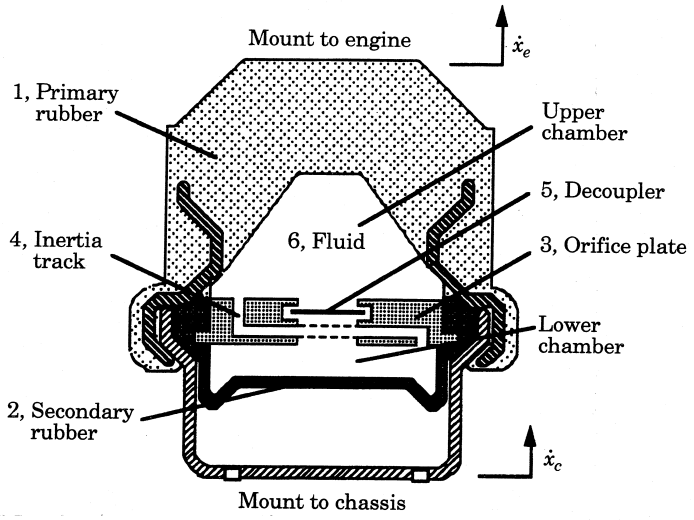

Figure 1. A schematic of a hydraulic engine mount.

Change has also been forced by an increased market emphasis on passenger comfort. Comfort encompasses interior noise and vibration as well as the feel of the vehicle on rough roads and under extreme acceleration. This serves only to heighten the conflicts that arise in design.

To meet the conflicting requirements of isolation and control, the automotive industry has turned increasingly to hydraulic engine mounts. A typical hydraulic mount is illustrated in Figure 1. To provide a basis for the design and analysis of such a mount, good models are essential. Toward this end, a variety of articles presenting mathematical models as well as design procedures has been published in the past decade [2–15]. An excellent review is provided by Singh *et al*. [11]. It should be noted that, while this paper focuses on passive engine mounts, a number of recent studies have explored semi-active or adaptive engine mounts as well [3, 10, 16–18].

Until recently, most attempts to model hydraulic mounts assumed linearity and were restricted to rather limited sets of operating conditions (usually corresponding to test conditions). Unfortunately, production hydraulic mounts exhibit a variety of non-linear characteristics and, in application, are subject to a broad range of excitations. The investigation of non-linear behavior appears to have begun with Ushijima and Dan [13], who used numerical simulation to investigate nonlinear flow characteristics. More recently, Kim and Singh [19, 20] began a systematic study of hydraulic mount non-linearities. Among the effects they have considered are non-linear compliance, non-linear flow characteristics, cavitation and "decoupling".

This paper contributes further to the understanding of mount non-linearity associated with the "decoupler". The decoupler, shown in Figure 1, is essentially an amplitude-dependent switch which is intended to improve the performance trade-off between vibration isolation and control of engine excursion.

Other contributions of this paper include the presentation of new experimental data describing the response of a hydraulic mount to composite, dual frequency excitations, as well as the presentation of a novel "small amplitude linear model". This linear model, developed as a preliminary to non-linear models, is the first in the literature to capture an important resonance associated with decoupler inertia. All models presented in this paper consider single axis excitation only, though extension to multiple axes is possible.

2. HYDRAULIC ENGINE MOUNT CHARACTERISTICS

2.1. PHYSICAL CHARACTERISTICS

In Figure 1, $x_e(t)$ and $x_c(t)$ represent the displacement of the engine and the chassis, respectively. The relative displacement, $x_0(t) = x_e(t) - x_c(t)$, is referred to as the "excitation" of the moment. Physical components which contribute significantly to the dynamics of the mount include the following. The primary rubber (1) is a rubber cone that serves several purposes. It support the static load of the engine, it contributes (significantly) to the elastic rate and (modestly) to the damping of the mount and it serves as a piston to pump fluid through the rest of the mount. The bulge rate of the primary rubber (ratio of pressure change to volume change) is also an important design parameter. The secondary rubber (2) is a rubber septum that serves principally to contain the fluid. It also contributes modestly to the elastic rate. The orifice plate (3) is a metal plate (actually a sandwich of two plates) that separates the "upper chamber" (enclosed by the primary rubber) and the "lower chamber" (enclosed by the secondary rubber). Cast in the orifice plate are the "inertia track" and "decoupler orifice." The inertia track (4) is a lengthy spiral channel that enables fluid to pass from the upper chamber to the lower chamber. The fluid inertia in this channel is significant, and is usually selected so that it experiences resonance at the natural frequency of the engine/mount system. The damping of the track is also significant. Thus, the inertia track acts as a tuned damper, and is introduced for the purpose of control. The decoupler (5) is a plastic plate which acts as an amplitude-limited floating piston that provides a low resistance path between the upper and lower chambers. Thus, for small amplitude excitation, most of the fluid transport between chambers is via the decoupler orifice, which effectively short-circuits the inertia track. For larger amplitude excitations, the decoupler "bottoms out" and most of the fluid flow is forced through the inertia track. The inertia of the decoupler is also important at high frequencies, a point which will be highlighted in this paper. The fluid (6), ethylene glycol, completely fills the interior of the mount.

2.2. FREQUENCY RESPONSE CHARACTERISTICS

The behavior of an engine mount is usually reported in terms of its frequency response for different amplitude excitations. Frequency/amplitude ranges of greatest interest include [6, 11, 14]: (1) 5–15 Hz, 0.5–5.0 mm—these excitations are in the range of engine resonance and large enough to require significant damping; (2) 25–250 Hz, 0.05–0.5 mm—these excitations can cause noise and vibration, and require good isolation. Even higher frequency excitations, which may result from combustion noise [14], have received attention recently, but are beyond the scope of this paper. Interest has also arisen in the extent to which hydraulic mounts can provide control and isolation *simultaneously* [14]. This may be important, for instance, while driving on rough surfaces, or during extreme accelerations on smooth surfaces. Thus, the response to composite inputs is of interest, and will be considered in this paper.

The frequency response is typically evaluated with a conventional servo-controlled hydraulic test rig. The chassis bracket is fixed to an inertially grounded force sensor, while the engine bracket is sinusoidally excited at a fixed amplitude. Force and displacement records are collected at a series of frequencies and each record is transformed to the frequency domain via a discrete Fourier transform. For this study, time domain records all consist of 8192 points collected at a sample interval of 0·0005 s. To analyze high frequency behavior (5–200 Hz increments), each record is broken into four contiguous sections which are independently windowed (Hanning window) and transformed. The four transforms are then ensemble-averaged to obtain estimates of the Fourier transform

and coherence. To analyze low frequency behavior (1–40 Hz in 1 Hz increments), each record is broken into eight interleaved sections (each with an effective sample rate of 0.004 s), which are independently windowed and transformed, then ensemble-averaged.† In all cases, only those data corresponding to the excitation frequency, ω, are retained. Coherences obtained in this way are not reported because they are in all cases extremely close to unity. The Fourier transforms, $F(j\omega)$ and $X_0(j\omega)$, correspond to the *fundamental harmonics* of force and displacement. The ratio of these transforms, known as the "dynamic stiffness" is the principal quantity of interest:

$$K_{dyn}(j\omega) = F(j\omega)/X_0(j\omega) = K(\omega) + j\omega B(\omega). \tag{1}$$

The real part of the dynamic stiffness, $K(\omega)$, is termed the "elastic rate", while the imaginary part divided by frequency, $B(\omega)$, is termed the "damping". In comparing these data with others in the literature, it should be noted that dynamic stiffness is often presented in terms of the magnitude ("dynamic rate") and phase ("loss angle").

Figure 2 shows representative data corresponding to the two classes of excitation considered above. The two curves correspond to 0.1 and 1.0 mm excitations. These data, as all comparable data in this paper, have been normalized by the stiffness and damping of the primary rubber (which are assumed to be amplitude and frequency-independent). It is clear that the response of the hydraulic mount is strongly amplitude-dependent.

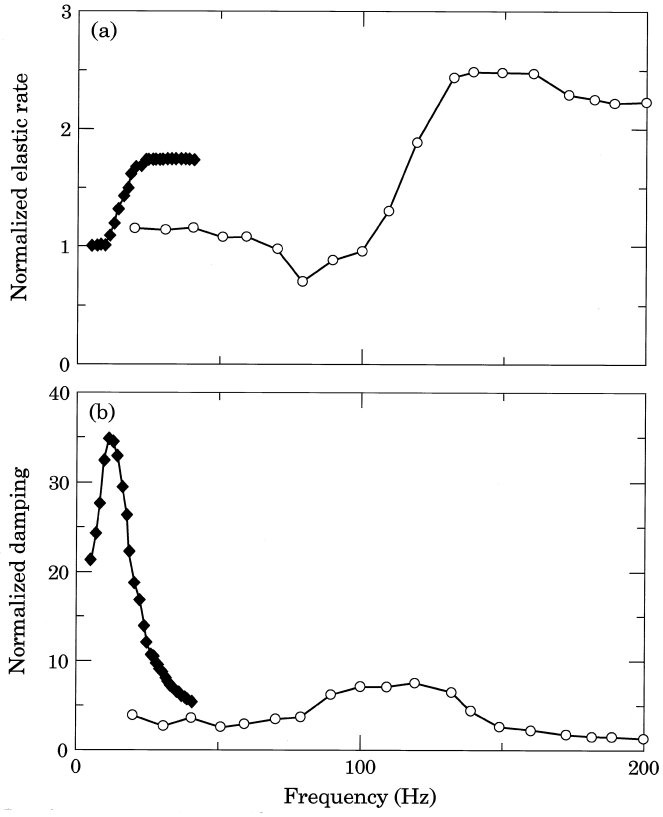

Figure 2. (a) Normalized elastic rate and (b) damping of a production hydraulic mount for small amplitude (—○—, 0·1 mm) and large amplitude (—◆—, 1·0 mm) excitations.

† Computational details are given in reference [21].

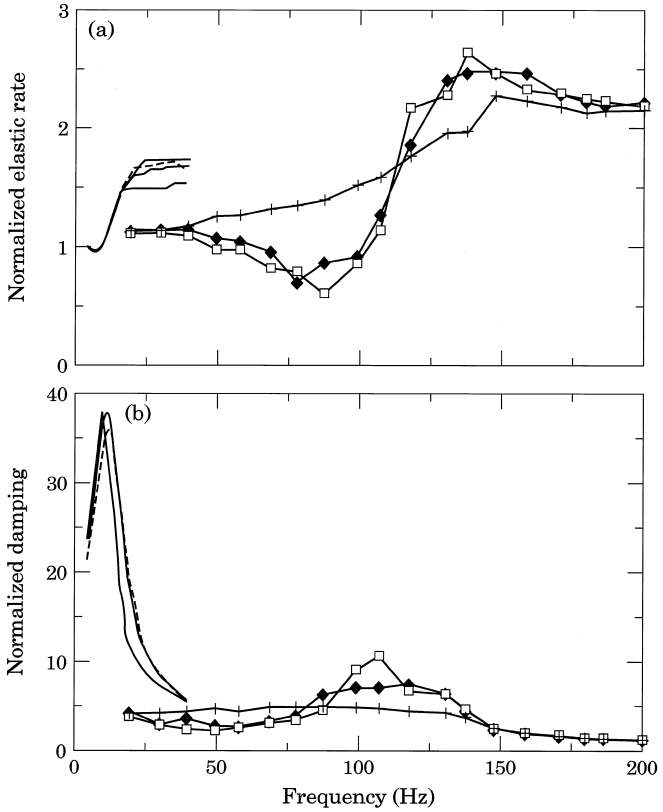

Figure 3. (a) Normalized elastic rate and (b) damping of a production hydraulic mount for various amplitudes: —□—, 0·05 mm; —◆—, 0·1 mm; —+—, 0·2 mm; ——, 0·4 mm; ——, 0·6 mm; ———, 0·8 mm; –·–·–·–, 1·0 mm.

The following points are also noteworthy: (1) the peak in the damping for large amplitude excitation ($\sim$15 Hz) has been "tuned" so that it corresponds to the natural frequency of engine bounce, thus, for large amplitude inputs, the mount serves as a tuned damper; (2) for frequencies less than $\sim$50 Hz, both the elastic rate and damping are much less for small amplitude inputs, resulting in superior vibration isolation; (3) the peak in damping for small amplitude excitation ($\sim$120 Hz) and the corresponding increase in elastic rate are the result of decoupler inertia, and are undesirable effects.

For this study, a more extensive set of data has been collected. These data are plotted in Figures 3–5. Figure 3 shows the response of the mount to different amplitude excitations. It is evident that, with increasing amplitude, the behavior shifts from the prototypical "small amplitude" response to the prototypical "large amplitude" response. The development of a model which captures this shift is a principal objective of this work.

Figure 4 displays frequency responses of three specially prepared engine mounts. The first is a mount from which the fluid was drained, leaving the primary rubber solely responsible for the dynamic behavior. The data show that the assumption of amplitude independence is very good, while the assumption of frequency independence is reasonable, but will introduce a certain degree of systematic error. The second specialty mount was assembled without a decoupler. The behavior is, not surprisingly, quite similar to the small amplitude response of a production mount. The third specialty mount had the decoupler fixed in place. The behavior resembles the large amplitude response of a production mount. These data are particularly useful in identifying model parameters.

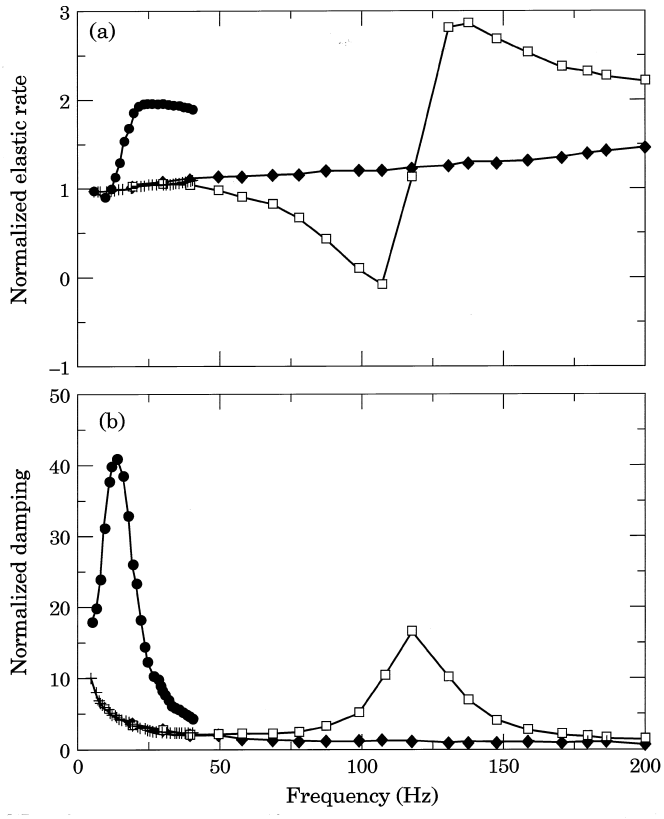

Figure 4. (a) Normalized elastic rate and (b) damping of three specially prepared engine mounts: —□—, mount with no decoupler, 0·05 mm; —●—, mount with fixed decoupler, 1·0 mm; —◆—, mount with no fluid, 0·05 mm; — + —, mount with no fluid, 1·0 mm.

Figure 5 displays frequency response of a production mount excited by composite waveforms:

$$x_0(t) = x_b(t) + x_s(t), \tag{2}$$

where

$$x_b(t) = 1{\cdot}0 \sin(2\pi\omega_b t)\ \text{mm}, \qquad \text{and} \qquad x_s(t) = 0{\cdot}1 \sin(2\pi\omega_s t)\ \text{mm}.$$

The "base frequency", ω_b of the large amplitude component is fixed for a given data set at 5, 10 or 15 Hz. The frequency, ω_s, of the small amplitude component is swept from 20 to 200 Hz. These data have been collected to assess the mount's capacity to provide isolation in the presence of a large amplitude disturbance. Toward this end, the relationship between the small amplitude input and the force is of particular interest.

The two frequencies, ω_b and ω_s, are generated by separate analog instruments, and therefore may be considered independent and uncorrelated [22]. This allows the computation of transfer functions relating each of these inputs to the output force:

$$K^b_{dyn}(\mathrm{j}\omega) = F(\mathrm{j}\omega)/X_b(\mathrm{j}\omega), \qquad K^s_{dyn}(\mathrm{j}\omega) = F(\mathrm{j}\omega)/X_s(\mathrm{j}\omega). \tag{3}$$

$F(\mathrm{j}\omega)$, $X_b(\mathrm{j}\omega)$ and $X_s(\mathrm{j}\omega)$ are Fourier transforms of their respective time domain records. It can be shown that transfer functions computed in this way are optimum

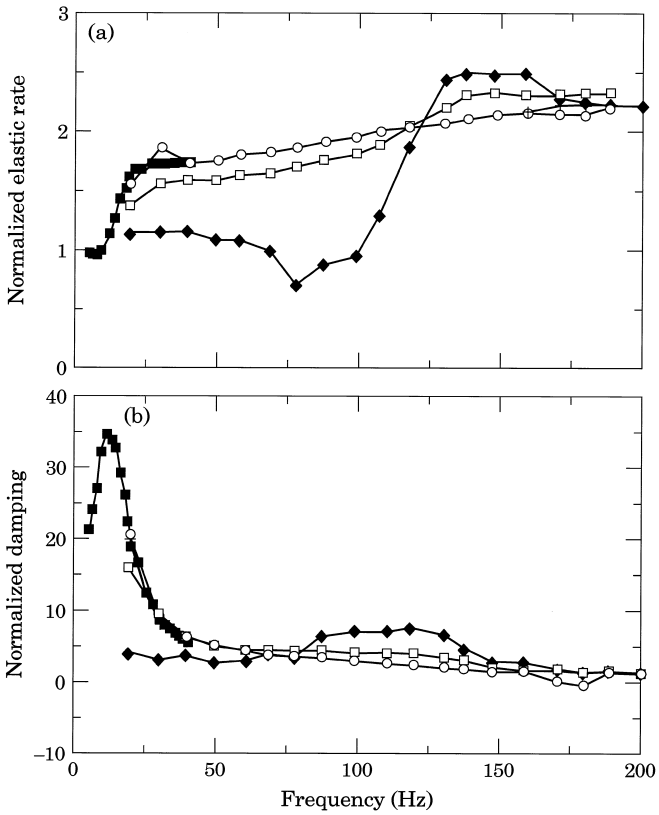

Figure 5. (a) Normalized elastic rate and (b) damping of a production mount excited by composite input consisting of a 1·0 mm sinusoid at a base frequency (5, 10, 15 Hz) and a 0·1 mm sinusoid (frequency on horizontal axis): —□—, 5 Hz base; —+—, 10 Hz base; —○—, 15 Hz base; —◆—, 0·1 mm single frequency response; —■—, 1·0 mm single frequency response.

linear approximations to the underlying non-linear system [22]. Because we are interested specifically in the response to small amplitude inputs, only the value of $K^s_{dyn}(j\omega)$ corresponding to the excitation frequency ω_s is retained. The coherence associated with this value approaches unity.

The results are quite interesting. They indicate that $K^s_{dyn}(j\omega)$ measured in the presence of a large amplitude disturbance bears a strong resemblance to the mount's large amplitude response (Figure 2). This implies that the mount's capacity to provide isolation from small amplitude, high frequency inputs is significantly degraded by the simultaneous presence of a large amplitude, low frequency disturbance. A similar conclusion was reached by Ushijima *et al*. [14] who performed a similar experiment.

2.3. MODEL REQUIREMENTS

The data described above give a more complete picture of hydraulic mount behavior than previously available. Based on them, it seems reasonable to assert that a good mount model should be able to capture: the low frequency, large amplitude resonance (which describes the mount's performance as a tuned damper); the high frequency, small amplitude resonance (which, though undesirable, figures prominently in the mount's performance as an isolator); the amplitude dependence of elastic rate and damping; and

the mount's response to composite inputs (which measures the mount's ability to provide simultaneous isolation and control).

The next section introduces two linear models. These models embody our basic physical understanding of the hydraulic mount, and are sufficient to capture the two resonances. Section 4 presents two approaches to estimating non-linear frequency responses, a piecewise linear simulation and an equivalent linearization analysis. These techniques are also extended to predict the mount's response to composite inputs. Section 5 presents a summary discussion.

3. LARGE AND SMALL AMPLITUDE LINEAR MODELS

In this section, two linear models are introduced. The first is tailored to large amplitude sinusoidal excitation ($>0{\cdot}5$ mm), and makes the assumption that the decoupler is "bottomed out" at all times. The second is tailored to small amplitude excitation ($<0{\cdot}5$ mm), and makes the assumption that the decoupler never bottoms out. Both models assume that all other important physical effects may be represented by lumped, linear time-invariant elements.

3.1. LARGE AMPLITUDE MODEL

The principal physical effects are taken to be those associated with the primary rubber (shear stiffness and damping; bulge stiffness; piston area) and with the inertia track (fluid inertia and damping). The stiffness of the secondary rubber is small enough that it can be ignored (reducing the requisite state dimension by one).† The fluid is assumed incompressible (the bulge compliance of the primary rubber is much greater), and the fluid inertia and damping in the upper chamber are ignored (inertia and damping in the track are much greater). The interconnection of these elements is straightforward—both bond graph [23, 24] and mechanical equivalent models are shown in Figure 6. Similar models have been presented in references [2, 5, 7, 11, 14].

State equations and an output equation for the reaction force may be derived from the bond graph. They are

$$\begin{bmatrix} \dot{x}_r \\ \dot{V}_b \\ \dot{Q}_t \end{bmatrix} = \begin{bmatrix} 0 & 0 & 0 \\ 0 & 0 & -1 \\ 0 & K_b/I_t & -B_t/I_t \end{bmatrix} \begin{bmatrix} x_r \\ V_b \\ Q_t \end{bmatrix} + \begin{bmatrix} 1 \\ A_p \\ 0 \end{bmatrix} \dot{x}_0, \tag{4}$$

$$F = [K_r \quad A_p K_b \quad 0] \begin{bmatrix} x_r \\ V_b \\ Q_t \end{bmatrix} + [B_r]\dot{x}_0.$$

The states are shear displacement of the primary rubber (x_r), bulge displacement of the primary rubber (V_b) and volumetric flow in the inertia track (Q_t).

Parameter values were obtained as follows. A_p, the "piston area" of the primary rubber, is equal to the area of the orifice plate top surface, which is easily measured. Initial estimates of bulge stiffness, K_b, track inertia, I_t, and track damping, B_t, were made using the analytical formulas given in Singh *et al*. [11]. These formulas, however, are necessarily

† This may be understood by comparing the response of the mount without fluid to the responses of the fluid-filled mounts. At low frequency, both rubber shear stiffness and secondary rubber stiffness should contribute to the elastic rate of the latter class; yet, these mounts exhibit nearly the same values as the dry mount (Figure 4). Measurements of primary rubber bulge compliance and secondary rubber compliance presented by Kim and Singh [20] also indicate that the latter is at least an order of magnitude greater.

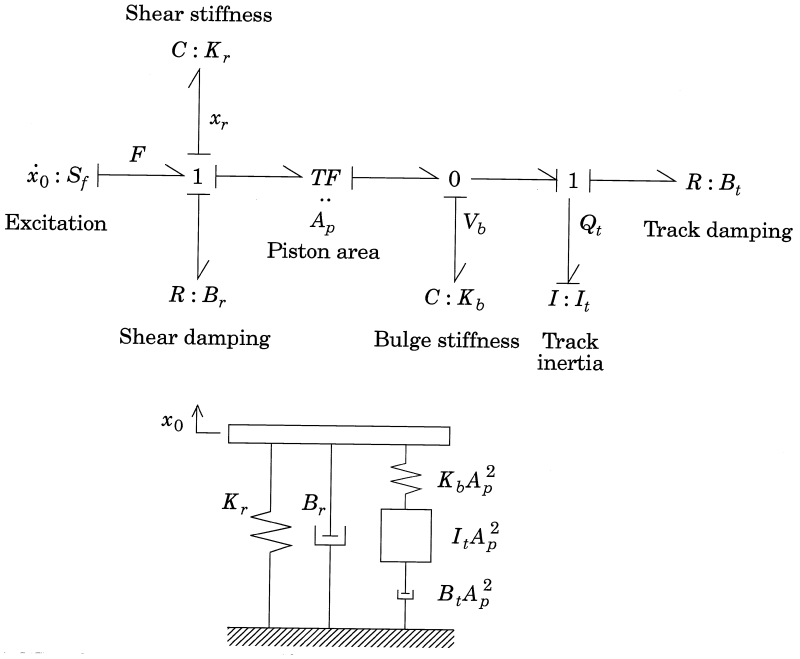

Figure 6. The large amplitude model.

based on idealized geometries, such as straight inertia track and a hemispherical upper chamber. Also idealized are the assumptions of laminar and fully developed flow through the inertia track. Finally, even such basic assumptions as the absence of leakage paths tend to short-circuit the inertia track may be questionable. Thus, analytically determined parameters must generally be considered no better than order-of-magnitude estimates. In this study, more accurate estimates of K_b, I_t and B_t, as well as primary rubber shear stiffness, K_r, and damping, B_r, were obtained from the frequency responses of the specialty mounts.

The specialty mount containing no fluid gives a direct measure of K_r and B_r. Though these parameters vary somewhat with frequency and excitation amplitude (Figure 4), representative values are selected and used in all models. These values are also used to normalize the elastic rate and damping plots.

The specialty mount with fixed decoupler should behave very much as the large amplitude model would predict; thus, it is useful for estimating K_b, I_t and B_t. These estimates are obtained by relating characteristics of the frequency response measurements to model predictions. The transfer function associated with the large amplitude model (equation (4)) is:

$$K_{dyn}(s) = \frac{F(s)}{X(s)} = K_r + B_r s + A_p^2 K_b \frac{I_t s^2 + B_t s}{I_t s^2 + B_t s + K_b}. \tag{5}$$

It is convenient to define a natural frequency and damping ratio associated with the fluid part of the system:

$$\omega_n = \sqrt{K_b / I_t}, \qquad \zeta = B_t / 2\sqrt{K_b I_t}. \tag{6}$$

The frequency response may then be written in terms of real (elastic rate) and imaginary (damping) parts:

$$K_{dyn}(j\omega) = \left[K_r + A_p^2 K_b \frac{\omega^2(\omega^2 - \omega_n^2) + 4\zeta^2\omega_n^2\omega^2}{(\omega^2 - \omega_n^2)^2 + 4\zeta^2\omega_n^2\omega^2} \right] + j\omega \left[B_r + A_p^2 K_b \frac{2\zeta\omega_n^3}{(\omega^2 - \omega_n^2)^2 + 4\zeta^2\omega_n^2\omega^2} \right], \quad (7)$$

At frequencies well above ω_n (>30 Hz), the elastic rate approaches $K_r + A_p^2 K_b$. Because K_r and A_p are known, this measure of elastic rate may be used to estimate bulge stiffness. In addition to the high frequency elastic rate, salient and reproducible features of the data are the resonant frequency, ω_{r1}, at which the peak in damping occurs, and the slope of the elastic rate curve at resonance, m_{r1} (see also Figure 7). These measures may be used to estimate ζ and ω_n, from which I_t and B_t can be determined. An expression for ω_{r1} is found by maximizing the damping term in equation (7):

$$\omega_{r1}^2 = \omega_n^2(1 - 2\zeta^2). \quad (8)$$

An expression for m_{r1} is found by differentiating the elastic rate term in equation (7), and evaluating at $\omega = \omega_{r1}$:

$$m_{r1} = (A_p^2 K_b / 2\omega_{r1})((1 - 2\zeta^2)/\zeta^2(1 - \zeta^2)). \quad (9)$$

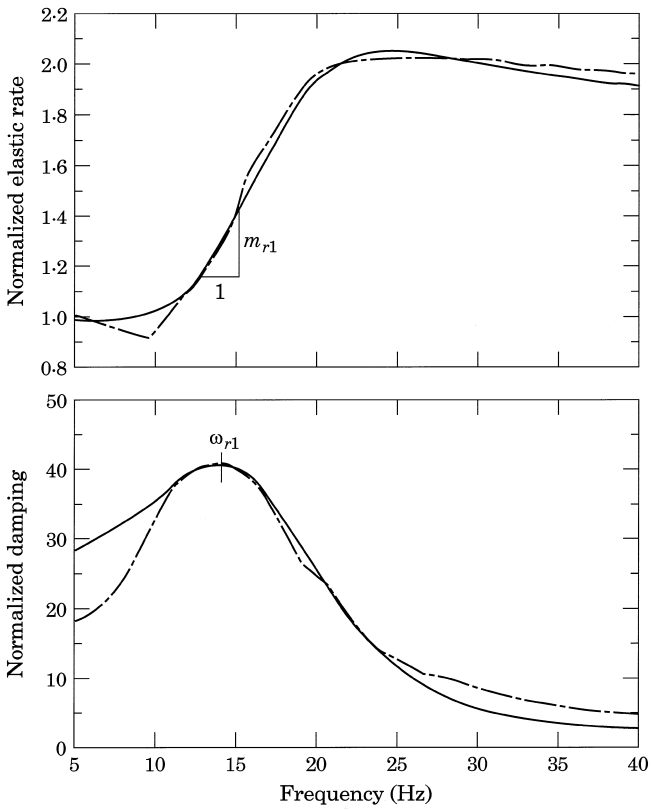

Figure 7. (a) Normalized elastic rate and (b) damping of large amplitude model versus data: ——, large amplitude model; – – –, mount with fixed decoupler, 1·0 mm.

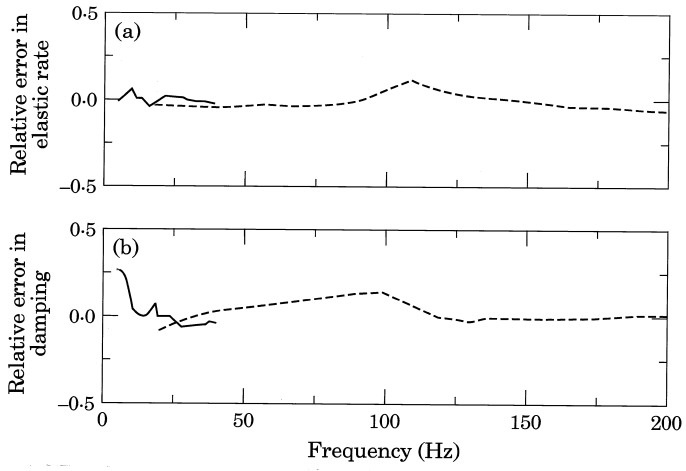

Figure 8. Relative errors of large amplitude and small amplitude linear models: ——, large amplitude, – – –, small amplitude. (a) Elastic rate; (b) damping.

Given measurements of ω_{r1} and m_{r1}, equation (9) may be used to estimate ζ: subsequently, equation (8) may be used to estimate ω_n. Determination of I_t and B_t is then straightforward, completing the parameter identification process. The frequency response of the identified large amplitude model is shown in Figure 7.

A quantitative measure of model performance is the frequency-dependent relative error, which for elastic rate will be defined as

$$\epsilon_K(\omega) = [\hat{K}(\omega) - K(\omega)]/\max_{\omega}(K(\omega)), \tag{10}$$

where $K(\omega)$ is the measured elastic rate and $\hat{K}(\omega)$ is the predicted elastic rate. The relative error in damping is defined analogously. These quantities are plotted in Figure 8 (along with those for the small amplitude model). Relative errors in elastic rate are generally less than 10%, while those in damping are less than 20%.

3.2. SMALL AMPLITUDE MODEL

The principal physical effects are taken to be those incorporated in the large amplitude model, plus those associated with the decoupler orifice (orifice inertia and damping). Figure 9 illustrates the model of decoupler orifice dynamics which is used. The decoupler itself and surrounding fluid are treated as a lumped inertia, I_0, while the fluid shear layer between this inertia and the orifice plate is treated as a lumped damper, B_0. The pressure drop between upper and lower chambers ($K_b V_b$, where V_b is the bulge displacement of the

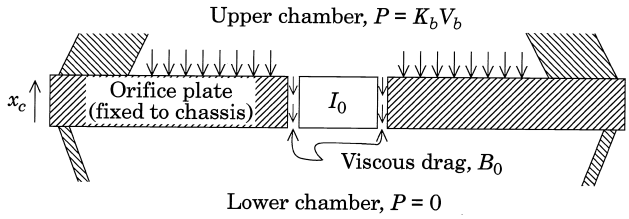

Figure 9. The orifice plate model.

primary rubber) drives the orifice flow, Q_0. A pressure balance gives

$$K_b V_b = I_0 \dot{Q}_0 + B_0(Q_0 - A_d \dot{x}_c). \tag{11}$$

A_d is the cross-sectional area of the orifice, and x_c is the displacement of the chassis, to which the orifice plate is fixed.

An expression for the force transmitted to the chassis can also be derived with the assistance of Figure 9. Contributions are the forces transmitted via rubber shear, the normal forces on the orifice plate due to pressure, and the shear forces due to drag:

$$F = K_r(x_e - x_c) + B_r(\dot{x}_e - \dot{x}_c) + (A_p - A_d)K_b V_b + (A_d^2 B_0)(Q_0/A_d - \dot{x}_c), \tag{12}$$

where x_e is the displacement of the engine.

The effect of orifice dynamics, as represented in equations (11) and (12), can be added to the large amplitude model by recognizing that the pressure drop across the inertia track is the same as that across the decoupler orifice. A complete small amplitude model is shown in Figure 10. A mechanical equivalent to this bond graph can be found, but is quite non-intuitive.

One interesting aspect of the small amplitude model is that it requires two inputs (x_e and x_c) rather than a single input ($x_0 = x_e - x_c$). The relative displacement is an appropriate input only in instances when either the engine or the chassis serves as an inertial ground and therefore a proper reference for the orifice inertia.† While no such instance occurs in an automobile, it does occur in the test fixture described in section 2.2 which fixes the chassis bracket to ground ($x_c = 0$). In this case, state and output equations are

$$\begin{bmatrix} \dot{x}_r \\ \dot{V}_b \\ \dot{Q}_t \\ \dot{Q}_0 \end{bmatrix} = \begin{bmatrix} 0 & 0 & 0 & 0 \\ 0 & 0 & -1 & -1 \\ 0 & K_b/I_t & -B_t/I_t & 0 \\ 0 & K_b/I_0 & 0 & -B_0/I_0 \end{bmatrix} \begin{bmatrix} x_r \\ V_b \\ Q_t \\ Q_0 \end{bmatrix} + \begin{bmatrix} 1 \\ A_p \\ 0 \\ 0 \end{bmatrix} \dot{x}_0, \tag{13}$$

$$F = [K_r \quad (A_p - A_d)K_b \quad 0 \quad A_d B_0] \begin{bmatrix} x_r \\ V_b \\ Q_t \\ Q_0 \end{bmatrix} + [B_r]\dot{x}_0.$$

All variables retain previous definitions. The only parameters which did not appear in the large amplitude model re A_d, I_0 and B_0.

The decoupler cross-sectional area is easily measured. Orifice inertia and damping can be estimated by a procedure similar to that used to find track inertia and damping. To simplify the analysis, it is first assumed that, at the frequency of orifice resonance ($\omega_2 \approx 120$ Hz), flow through the inertia track can be neglected. This simplification gives the dynamic stiffness of the small amplitude model a form very similar to equation (5):

$$K_{dyn}(s) = \frac{F(s)}{X(s)} = K_r + B_r s + A_p^2 K_b \frac{(1-\epsilon)I_0 s^2 + B_0 s}{I_0 s^2 + B_0 s + K_b}, \tag{14}$$

where $\epsilon = A_d/A_p$. Equation (14) may be used to develop expressions for the resonant frequency (ω_{r2}) and slope of the elastic rate plot at resonance (m_{r2}). These expressions may be equated to values measured using the speciality mount with no decoupler, and solved to yield estimates of I_0 and B_0. This process is similar to that used to estimate

† This is not an issue with the track inertia because flow in the track is perpendicular to the assumed axis of motion.

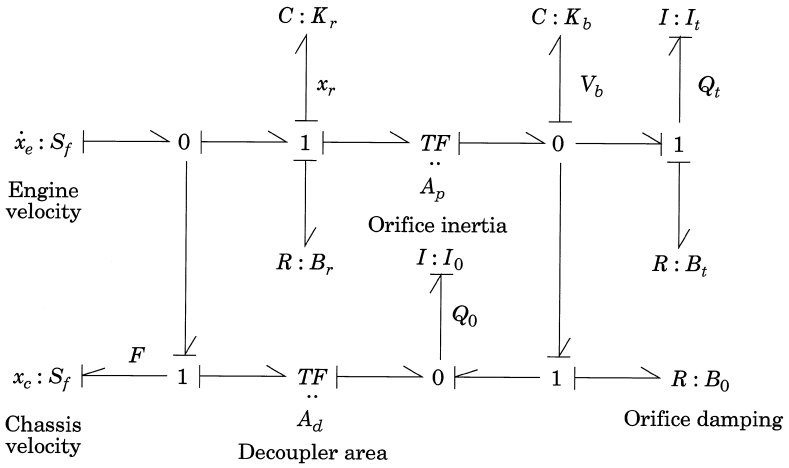

Figure 10. The small amplitude model.

I_t and B_t, but somewhat more involved due to the presence of ϵ. Details are given in Appendix A.

The frequency response of the fully identified small amplitude model is shown in Figure 11. Relative errors are shown in Figure 8, and are comparable to those of the large

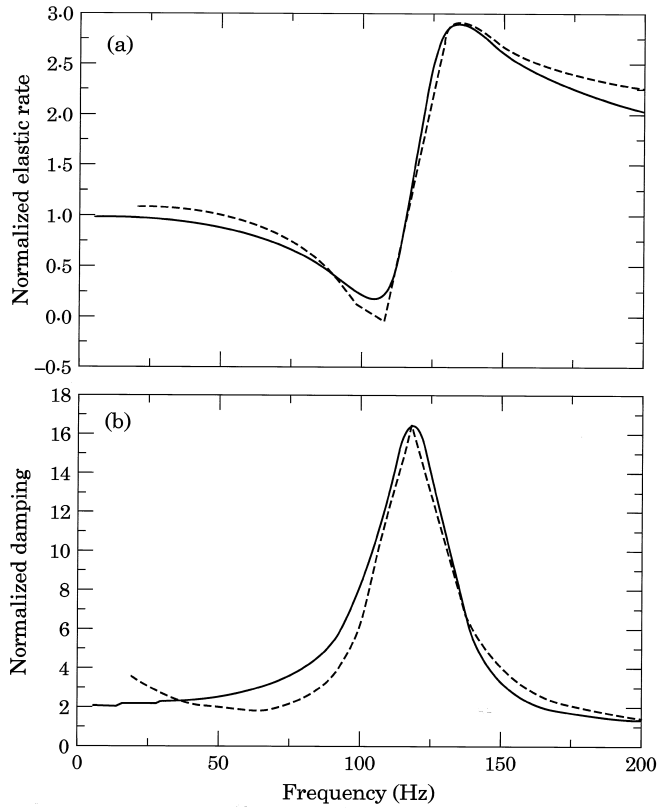

Figure 11. (a) Normalized elastic rate and (b) damping of small amplitude model versus data: ——, small amplitude model: – – –, mount with no decoupler, 0·05 mm.

magnitude model. Although the linear models successfully capture the two resonances, they cannot represent in any greater detail the amplitude dependence of the mount's response. To meet this objective, two non-linear models are introduced.

4. NON-LINEAR MODELLING

A variety of non-linear effects contributes significantly to the behavior of a production hydraulic mount [20]. These include, for instance, entrance and exit effects in the inertia track flow, and amplitude-dependent softening of the primary rubber. In this paper, however, attention will be focused on the decoupler, which is principally responsible for the amplitude dependence.

4.1. PIECEWISE LINEAR MODEL

A direct approach to incorporating decoupler behavior is via a piecewise linear model [19, 25]. In essence, the piecewise linear model reduces to the small amplitude linear model (augmented with a state for decoupler position, x_d) whenever the decoupler is not bottomed out, and to the large amplitude model when the decoupler is bottomed out. The behavior of the model can be investigated using numerical integration. The model developed in reference [25] uses the following scheme for switching during a time domain integration (δ is half the gap width):

If the previous step was integrated with the small amplitude model: if $|x_d| < \delta$, integrate small amplitude state equations; if $|x_d| \geqslant \delta$ and sign (V_b) = sign (x_d), set $Q_0 = 0$, set $x_d = \text{sign}\,(x_d)\delta$, and integrate large amplitude state equations.

If the previous step was integrated with the large amplitude model: if sign (V_b) = sign (x_d), integrate large amplitude state equations; if sign $(V_b) \neq$ sign (x_d), integrate small amplitude state equations.

Note that V_b is linearly related to the pressure in the upper chamber, which determines whether a decoupler at the limits of its travel will remain bottomed out or not.

A piecewise linear model has several attractive features. No new dynamic elements need be introduced to account for bottoming out, nor do the (possibly very fast) dynamics of the bottoming out process need to be directly considered. Moreover, the linear continuous state equations can be directly mapped to difference equations which are guaranteed stable [26], so that an efficient simulation can be performed. Finally, excitations of arbitrary shape are easily accommodated.

A significant disadvantage, however, is that a tremendous amount of time domain simulation data must be generated to produce a modest amount of frequency domain data. Frequency responses have been computed as follows. A sinusoidal excitation of amplitude X_0 and frequency ω is assumed. A simulation time increment of $2\pi/\omega/64$ seconds is picked, and time domain records of approximately 1150 points are computed. Records include position input and force output information. The beginning of each record is cut off to remove the transient response, leaving a record of 1024 points. This record is broken into three overlapping sections of 512 points each, which are Hanning windowed and transformed with an FFT. A complex transfer function is computed at the frequency of excitation.

Results are shown in Figure 12 (which may be compared with Figure 3), and relative errors in Figure 13. Generally speaking, the simulation is quite accurate. Relative errors in elastic rate and damping are typically less than 20%. The greatest errors occur in the vicinity of the high frequency resonance, due both to noise in the measured values and to poorness of fit. It is suspected that the poor fit near resonance is due to the lack of an appropriate model of the bottoming out process. This is addressed further below, but it

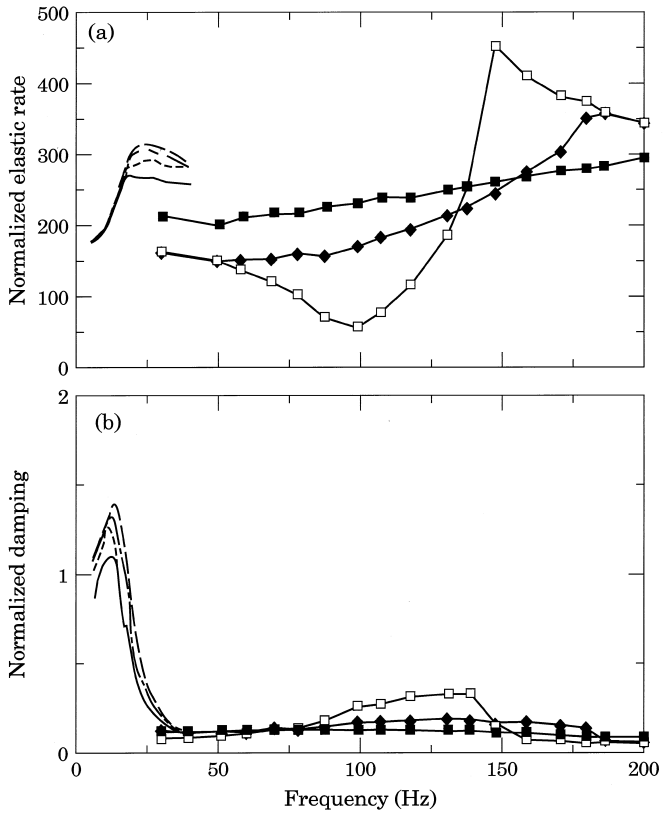

Figure 12. (a) Normalized elastic rate and (b) damping of piecewise linear model for various amplitude excitations. Compare with Figure 3: —□—, 0·05 mm; —◆—, 0·1 mm; —■—, 0·2 mm; ——, 0·4 mm; – – –, 0·6 mm; –·–·–·–, 0·8 mm; – – – –, 1·0 mm.

should be noted here that limited insight into bottoming out is a significant weakness of the piecewise linear model.

4.2. EQUIVALENT LINEARIZATION

An alternative approach to non-linear modelling, equivalent linearization, provides roughly comparable results (to piecewise linear modelling) at a greatly reduced computational cost, and with the added benefit of improved physical insight. Equivalent linearization techniques have been applied to similar problems with considerable success (see, for instance, Dubowsky and Freudenstein [27] and Comparin and Singh [28]). To introduce the technique, the simplified mechanical system in Figure 14 will first be considered. Note that the mass representing decoupler inertia is constrained by a "cage".

The idea of equivalent linearization is, given a prescribed excitation (e.g., $x_0(t) = X_0 \sin \omega t$), to replace the cage with a linear element or elements that would yield the same motion, at least up to the fundamental of the Fourier series describing that motion. The equivalent linear element(s) are then, in effect, parameterized by the amplitude and frequency of excitation.

The specific approach taken here is illustrated in Figure 15. As the figure indicates, only one element, the viscous damper, is affected by equivalent linearization. There is some physical justification for this model. First, there is no physical reason to associate

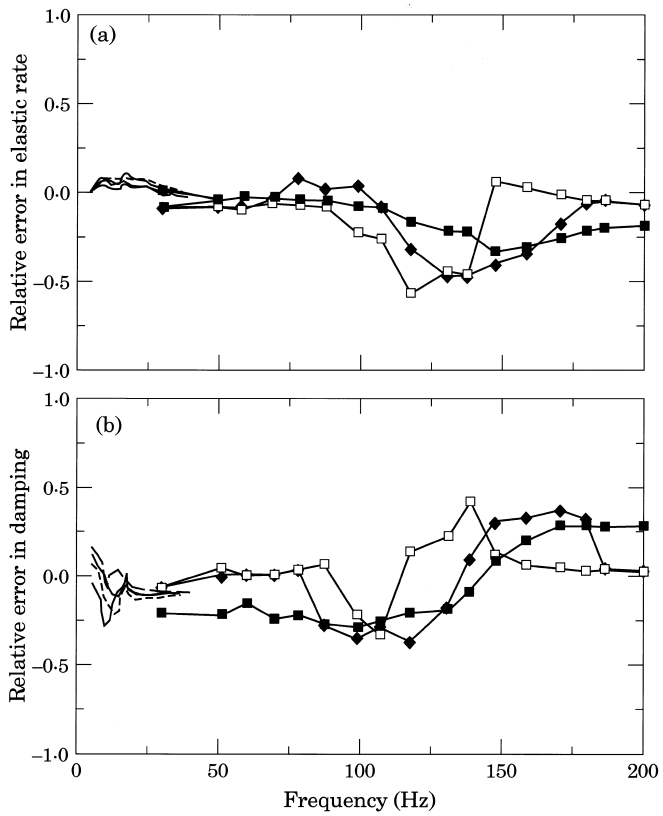

Figure 13. Relative errors for piecewise linear model: —□—, 0·05 mm; —◆—, 0·1 mm; —■—, 0·2 mm; ——, 0·4 mm; ----, 0·6 mm; –·–·–·–, 0·8 mm; – – – –, 1·0 mm. (a) Elastic rate; (b) damping.

significant energy storage (potential or kinetic) with bottoming out. Second, the decoupler is immersed in a fluid which must be displaced as the cage boundaries are approached. Thus, a squeeze film [29] is developed. It is well-known that the squeeze film between parallel plates produces a damping force which varies as the inverse cube of the gap [29, 30]:

$$F_{sq} = \gamma(\dot{h}/h^3) \tag{15}$$

Here, h is the gap thickness and γ is a geometric parameter. For simple geometries, equation (15) is readily derived from the Reynolds equation for viscous flow [30]. The geometry of decoupler/cage interaction is not simple, but it has been assumed that the inverse cube form holds nonetheless. The implications of this assumption will be reassessed below. Because the cage in Figure 14 has two sides, the appropriate damping

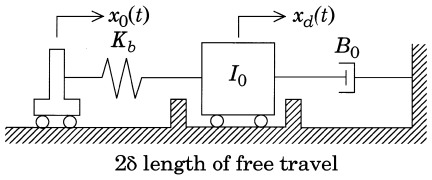

Figure 14. The simplified model.

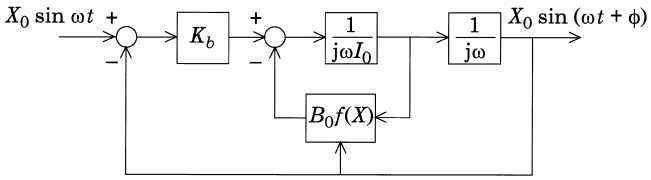

Figure 15. The model which treats the decoupler cage as an amplitude-dependent dissipator.

relation is

$$F_{sq}(x_d, \dot{x}_d) = \gamma\left[\frac{1}{(\delta - x_d)^3} + \frac{1}{(\delta + x_d)^3}\right]\dot{x}_d, \qquad F_{sq}(\bar{x}, \dot{\bar{x}}) = \beta\delta\left[\frac{1 + 3\bar{x}^2}{(1 + \bar{x}^2)^3}\right]\dot{\bar{x}}, \quad (16a, b)$$

where β is a geometric constant with units of damping and $\bar{x} = x_d/\delta$.

The non-linear damping relation of equation (16b) may be converted to an equivalent linear damping via a procedure outlined by Gibson [31]. To begin, assume that $\bar{x} = a \sin \omega t$. Then the force that results from equation (16b) can be represented by a Fourier series:

$$F_{sq}(a \sin \omega t, a\omega \cos \omega t) = F_0 + K_{eq}\delta a \sin \omega t + B_{eq}\delta a\omega \cos \omega t + \text{higher harmonics}. \quad (17)$$

It is easily shown that the constant term (F_0) and in-phase component of the fundamental ($K_{eq}\delta a$) are zero. Ignoring higher order harmonics, the equivalent behavior is that of a viscous damper with an amplitude-dependent coefficient,

$$B_{eq}(a) = \frac{\beta}{\pi}\int_0^{2\pi} \frac{\cos^2 u(1 + 3a^2 \sin^2 u)}{(1 - a^2 \sin^2 u)^3}\,\mathrm{d}u, \quad (18)$$

where $u = \omega t$. It is interesting to note that this amount of viscous damping would ensure precisely as much energy dissipation per cycle as the squeeze film damper, *assuming the same sinusoidal form for* $\bar{x}$. This function is plotted in Figure 16. Note that

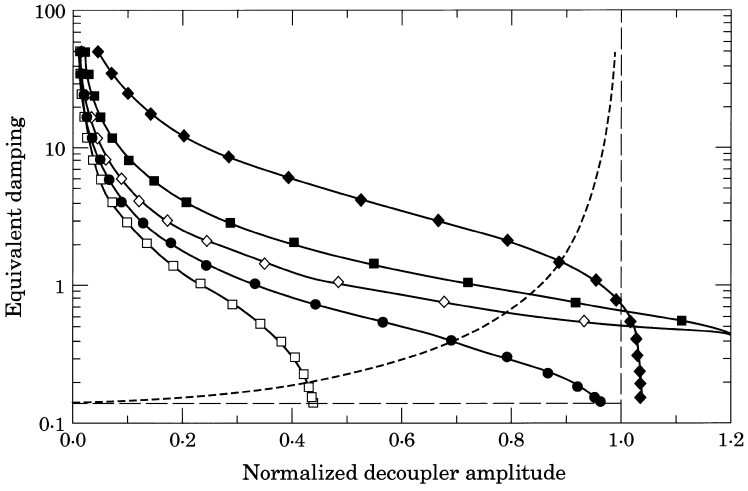

Figure 16. Equivalent damping as a function of normalized decoupler amplitude (equation (18)): ——. Effect of equivalent damping on normalized decoupler amplitude, assuming fixed excitation amplitude (equation (19)): —◆—, $\omega = 0{\cdot}2$; —■—, $\omega = 0{\cdot}6$; —◇—, $\omega = 1{\cdot}0$; —●—, $\omega = 1{\cdot}4$; —□—, $\omega = 1{\cdot}8$; where ω is normalized frequency. Simplified form of $B_{eq}(a)$ ———.

the equivalent damping approaches infinity as the normalized decoupler amplitude, a, approaches 1.

If $B_0 f(x)$ in Figure 15 is replaced with B_{eq}, a transfer function may be found relating $X(j\omega)$ to $X_0(j\omega)$. The magnitude of this transfer function can be considered an expression for the normalized decoupler amplitude in terms of equivalent damping, excitation amplitude and frequency:

$$a(B_{eq}, X_0, \omega) = \frac{X}{\delta} = \frac{K_b}{\sqrt{(K_b - I_0\omega^2)^2 + (B_{eq}\omega)^2}} \frac{X_0}{\delta}. \tag{19}$$

This relation has been plotted in Figure 16 for a single value of X_0 and several frequencies. Given specific values for X_0 and ω, equations (18) and (19) may be considered simultaneous equations to be solved for a and B_{eq}. This solution corresponds to a point of intersection in Figure 16. It is evident that, at each frequency, only one intersection will be found; thus, a uniquely defined frequency response will be computed (the uniqueness of the result can be proven rigorously [32]). The result is shown in Figure 17.

This same technique has been used to compute the frequency response of the hydraulic mount at various amplitudes. The linear orifice damping of the small amplitude model is replaced by the squeeze film damping of equation (16), with $\beta = B_0$ (thus, for an infinitesimal excitation, the non-linear model reduces to the small amplitude linear model).

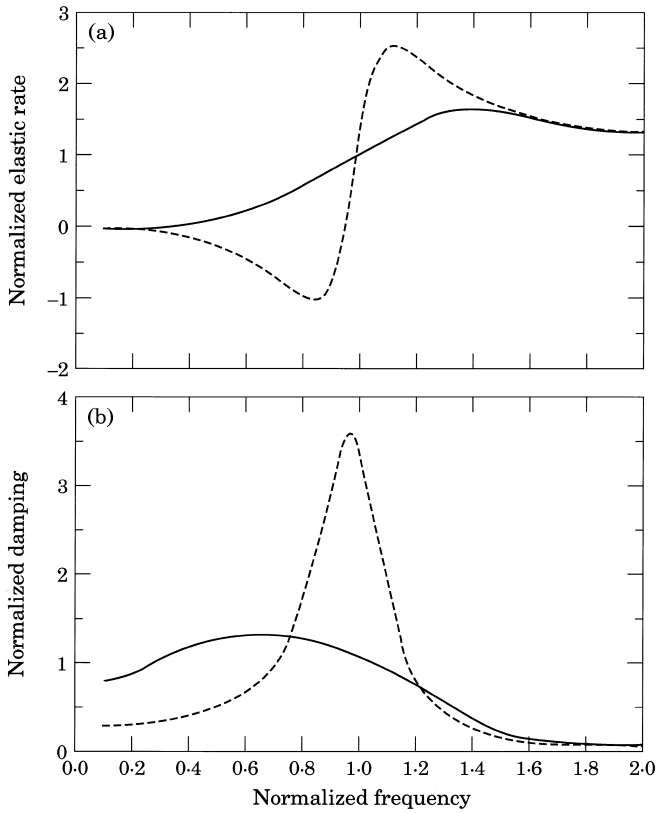

Figure 17. Frequency response —— of the system in Figure 14 treating the cage as an amplitude-dependent dissipator (Figure 15). Small amplitude (linear) frequency response ——. (a) Elastic rate; (b) damping.

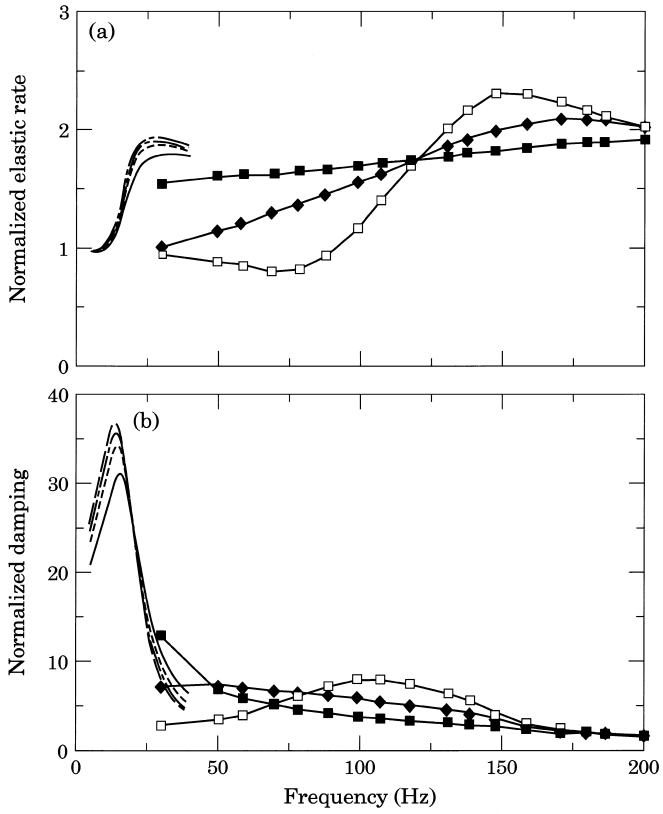

Figure 18. Normalized elastic rate and damping of equivalent linear model for various amplitude excitations. Compare with Figure 3: —□—, 0·05 mm; —◆—, 0·1 mm; —■—, 0·2 mm; ——, 0·4 mm; ----, 0·6 mm; –·–·–·–, 0·8 mm; — — —, 1·0 mm. (a) Elastic rate; (b) damping.

The results are shown in Figure 18 (compare with Figure 3), and the relative errors in Figure 19. Equivalent linearization proves, in fact, to be superior to the piecewise linear model for high frequency inputs, but poorer for low frequency, large amplitude inputs. The former point is expected, because equivalent linearization treats the bottoming out process in a more physically meaningful way and because, at high frequency, the assumption of sinusoidal decoupler motion is qiute reasonable. By the same token, the latter point may be understood: for large amplitude, low frequency inputs, the decoupler motion is nearly a square wave, and the force generated by the squeeze film is dominated by pulses which occur as the decoupler approaches and departs the cage limits. Indeed, most of the energy of the force signal is then found in the fifth and higher harmonics.

4.3. THE EFFECT OF HIGHER HARMONICS

Given the amount of spectral information which is lost, it may be surprising that the equivalent linearization technique works as well as it does. This is in part because comparison is being made to experimental data which has been analyzed in a similar way, ignoring higher harmonics in the force data. A second reason of importance, however, may be that the measured force is affected principally by the pressure in the upper chamber,

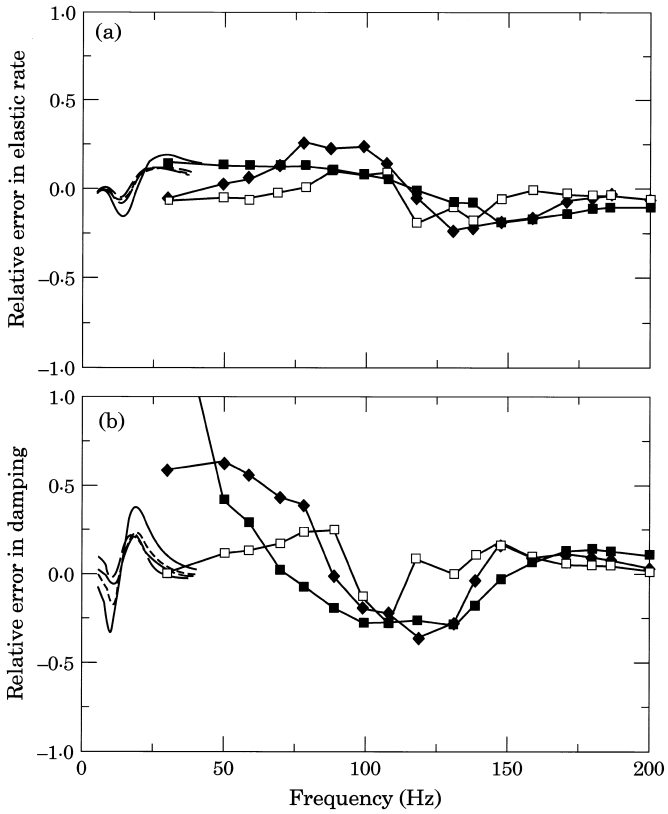

Figure 19. Relative errors of equivalent linear model: —□—, 0·05 mm; —◆—, 0·1 mm; —■—, 0·2 mm; ——, 0·4 mm; – – –, 0·6 mm; –·–·–·–, 0·8 mm; — — —, 1·0 mm. (a) Elastic rate; (b) damping.

not the pressure in the squeeze film; moreover, while higher harmonics may contribute significantly to the latter, they do not to the former.†

To illustrate these points, the various effects contributing to measured force may be estimated and compared. The greatest effect, in response to low frequency, large amplitude excitations, is upper chamber bulge caused by the imposed displacement. The magnitude of this effect is

$$F_1 \approx A_p^2 K_b X_0. \tag{20}$$

This force is purely sinusoidal, contributing no harmonics. There are two effects associated with the decoupler. The first is associated with the amount of upper chamber bulge caused by decoupler motion. At low frequency the decoupler motion will approximate a rectangle wave; therefore, the associated force will exhibit harmonics. The magnitude of the nth harmonic will be approximately proportional to $1/n$ for the first few harmonics. Higher harmonics will be even smaller because the decoupler motion is smooth rather than truly rectangular. The force contributed by a lower harmonic will be, approximately,

$$F_2 \approx A_p K_b (A_d(\delta/n)). \tag{21}$$

The magnitude of this effect is much smaller than F_1. For the fundamental, $F_2/F_1 \approx 0{\cdot}1$, given a 1 mm excitation amplitude.

† Shear force in the rubber contributes heavily to the measured force as well, but is relatively simple to describe and not particularly interesting in the present discussion.

The second force term is associated with decoupler inertia. This term is simply decoupler mass times acceleration, which, for the nth harmonic, is of the order

$$F_3 \approx (I_0 A_d^2)(\delta/n)(n\omega)^2 \approx A_p^2 K_b \epsilon^2 n\delta(\omega/\omega_{r2})^2. \tag{22}$$

For $n = 5$ and $\omega = 30$ Hz, $F_3/F_1 \approx 5 \times 10^{-4}$. Thus, because the inertia of the decoupler is very small, contributions of squeeze film pressure pulses to the measured force are very small.

4.4. SIMPLIFIED FORM OF EQUIVALENT DAMPING

The point was made early in section 4.2 that no particularly compelling reason exists to assume that the squeeze film relation applies to a hydraulic mount. Results of the equivalent linearization analysis, however, support the idea that a reasonable physical picture of bottoming out includes amplitude-dependent damping. With this in mind, a simplified form of $B_{eq}(a)$, shown in Figure 16, was investigated. Here, the equivalent damping is set to B_0 unless the decoupler amplitude is observed to exceed its physical limits. In such a case, an equivalent damping is selected which is precisely large enough to ensure that the decoupler motion remains within limits. The results (not shown) are very similar to those obtained with squeeze film damping. This similarity suggests that the precise form of equivalent damping relation is not very important, as long as it conforms to the general shape seen in Figure 16.

4.5. COMPOSITE EXCITATIONS

A final objective of this work has been to predict the hydraulic mount's response to composite excitations of the form given in equation (2). This is straightforward with the piecewise linear model, but less so via equivalent linearization.

The use of the piecewise linear model remains exactly the same as with a single frequency, except that the input changes to that given in equation (2). As with the experimental data, the transfer function is computed at ω_s, the frequency of the small amplitude component, only. This focuses attention on the capacity of the mount to provide isolation in the presence of low frequency disturbances.

As in the experimental measurements, it is necessary to ensure that the two components of the excitation may be treated as statistically independent. Because the amplitude and frequency of each component are fixed, the phase angles must be independent. This will *not* be the case if the two sinusoids are harmonically related. Thus, in performing a simulation it is important to pick ω_b and ω_s carefully so that, to within machine precision, no harmonic relationship exists.

Results are presented in Figure 20, which has the same format as Figure 5. Both simulation and experiment suggest that the response to small amplitude inputs in the presence of a low frequency, large amplitude disturbance is roughly comparable to the response one would expect for large amplitude single frequency inputs (which of course cannot be readily generated at such high frequencies). It is not surprising that the piecewise linear simulation would predict this because it employs the large amplitude model whenever the decoupler is bottomed out; moreover, the large amplitude component of the excitation ensures that the decoupler is bottomed out a significant percentage of the time.

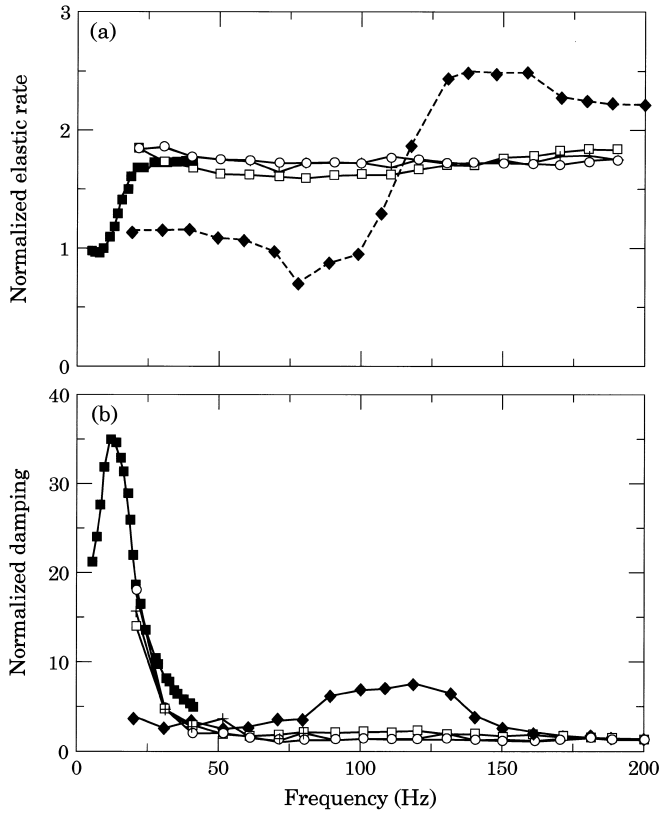

Figure 20. Response to composite excitations predicted by piecewise linear model. Compare with Figure 5. —□—, 5 Hz base; —+—, 10 Hz base; —○—, 15 Hz base; —◆—, 0·1 mm single frequency response; —●—, 1·0 mm single frequency response. (a) Elastic rate; (b) damping.

It is also instructive to use the equivalent linearization approach, which begins with the assumed decoupler motion (normalized)

$$\bar{x} = a_b \sin(\omega_b t + \phi_b) + a_s \sin(\omega_s t + \phi_s), \tag{23}$$

where $a_b + a_s < 1$. The equivalent linear behavior can be found using a double Fourier series [33], which has the form

$$6F_{sq} = \sum_{m=0}^{\infty} \sum_{\substack{n=-\infty(m\neq 0) \\ n=0(m=0)}}^{\infty} [P_{mn} \sin(mu_b + nu_s) + Q_{mn} \cos(mu_b + nu_s)], \tag{24}$$

where $u_b = \omega_b t + \phi_b$, $u_s = \omega_s t + \phi_s$. Note that many frequencies other than harmonics appear in the Fourier series. For instance, output frequencies of $\omega_s \pm \omega_b$, $\omega_s \pm 2\omega_b, \ldots, 2\omega_s \pm \omega_b$, $2\omega_s \pm 2\omega_b, \ldots$ can be expected. These terms are often called "combination tones" [34]. If the ratio of ω_s to ω_b is rational, then an infinite number of combination tones will occur at the frequencies of excitation. Thus, it is once again necessary to ensure that a harmonic relationship does not exist between the two sinusoidal components. Even so, combination tones will exist at frequencies close to excitation, and it is necessary to assume that they have minimal effect on the response. This assumption is supported in part by the reasoning presented in section 4.3.

It is readily shown that Q_{00}, P_{10} and P_{01} are all zero, while Q_{10} and Q_{01} are non-zero and are related to the equivalent damping at ω_b and ω_s, respectively:

$$B_b(a_b, a_s) = \frac{Q_{10}}{a_b\omega_b} = \frac{1}{2\pi^2}\int_{-\pi}^{\pi}\int_{-\pi}^{\pi}(\cos u_b + \frac{a_s\omega_s}{a_b\omega_b}\cos u_s) \times \frac{1 + 3(a_b \sin u_b + a_s \sin u_s)^2}{(1 - (a_b \sin u_b + a_s \sin u_s)^2)^3}\cos u_b \, \mathrm{d}u_b \, \mathrm{d}u_s$$

$$= \frac{1}{2\pi^2}\int_{-\pi}^{\pi}\int_{-\pi}^{\pi}\cos^2 u_b \frac{(1 + 3(a_b \sin u_b + a_s \sin u_s)^2}{(1 - (a_b \sin u_b + a_s \sin u_s)^2)^3}\,\mathrm{d}u_b \, \mathrm{d}u_s, \tag{25}$$

$$B_s(a_b, a_s) = \frac{Q_{01}}{a_s\omega_s} = \frac{1}{2\pi^2}\int_{-\pi}^{\pi}\int_{-\pi}^{\pi}\left(\frac{a_b\omega_b}{a_s\omega_s}\cos u_b + \cos u_s\right) \times \frac{1 + 3(a_b \sin u_b + a_s \sin u_s)^2}{(1 - (a_b \sin u_b + a_s \sin u_s)^2)^3}\cos u_s \, \mathrm{d}u_b \, \mathrm{d}u_s$$

$$= \frac{1}{2\pi^2}\int_{-\pi}^{\pi}\int_{-\pi}^{\pi}\cos^2 u_s \frac{(1 + 3(a_b \sin u_b + a_s \sin u_s)^2}{(1 - (a_b \sin u_b + a_s \sin u_s)^2)^3}\,\mathrm{d}u_b \, \mathrm{d}u_s. \tag{26}$$

These equations may be used, together with two transfer function relations similar to equation (19) (one at each frequency) to yield a set of four non-linear equations in four unknowns (B_b, B_s, a_b, a_s).

A very useful result can be obtained, however, without solving any sets of equations. It is readily shown by direct computation that $B_s > B_b$ whenever $a_b > a_s$. Clearly, we can expect that the latter condition holds because the excitation amplitude at the base frequency is ten times larger than that at the higher frequency. Moreover, the equivalent damping at the base frequency, B_b, must be large enough to limit the decoupler motion. As seen in the single frequency analysis, this ensures that the frequency response approaches that of the large amplitude model. The inequality in equivalent damping values then implies that the response at the higher frequency, ω_s, also approaches that of the large amplitude model. This is in agreement with the behaviors seen in Figures 5 and 20.

5. CONCLUSIONS

Novel experimental data and mathematical models describing a hydraulic engine mount have been presented. Piecewise linear and equivalent linear models have been shown to represent hydraulic mount behavior over a broader range of excitations than previously possible. While these results provide an excellent basis for hydraulic engine mount analysis and design, they also suggest a number of topics for future research.

For instance, while the large amplitude and small amplitude linear models fit the data remarkably well, the incorporation of certain additional effects, such as lower chamber compliance, upper chamber bulge damping and leakage past the decoupler, can lead to moderately improved fits [25]. More importantly, it is possible that some of these effects could be enhanced to improve the performance of future mount designs. For instance, a significant increase in upper chamber damping can be used to eliminate the high frequency resonant peak (with the cost, however, of higher damping at frequencies above resonance). Along similar lines, an interesting adaptive hydraulic mount was recently proposed by Kim and Singh [17]. This concept uses intake manifold vacuum and an electronic controller to switch the upper chamber compliance between high and low values according to vehicle operating conditions.

Non-linearities other than those associated with the decoupler, such as entrance and exit effects in the inertia track, may also exert a significant influence on the mount's behavior [20]. For instance, the over-estimation of damping at frequencies less than 10 Hz (Figure 7) is probably a consequence of having ignored such effects. Thus, future models should incorporate other non-linear effects.

The piecewise linear model presented here was particularly adept at capturing low frequency amplitude dependence while the equivalent linearization technique was adept at higher frequency. This was because the former did not incorporate a meaningful model of bottoming out, while the latter was incapable of representing substantially non-sinusoidal signals. A valuable contribution would be the development of a computationally efficient model combining the best characteristics of each. This is a challenge because higher order equivalent linearization techniques generally require the solution of sets of non-linear equations, while a simulation which represents bottoming out explicitly will be stiff.

The two models substantiated experimental results obtained with composite waveforms. The equivalent linearization technique, however, left open the tantalizing possibility that the mount's ability to provide simultaneous control and isolation could be improved with some other decoupler characteristic. This possibility has also been raised by Ushijima *et al*. [14], who argue that a rubber membrane decoupler gives better performance than a rigid plate decoupler, as considered here.

Finally, it would be inappropriate to close a discussion of hydraulic engine mounts without recalling the greater context. Engine mounts are but one contribution to the noise, vibration and harshness characteristics of an automobile. Hydraulic mounts, in particular, are designed for significant energetic interaction with the engine and chassis (as an example, the "apparent inertia" of the inertia track, $A_p^2 I_t$, is comparable to the engine mass). It is reasonable to expect, therefore, that the performance of a hydraulic mount will be sensitive to the dynamic characteristics of the vehicle in which it is placed. Moreover, performance must ultimately be considered a matter of subjective (passenger) impression. These factors have to date, and will for the foreseeable future, necessitate a rather lengthy cycle of design, testing and redesign. Thus, it is not simply the hydraulic mount itself, but its role in this broader context which must be the subject of future studies.

ACKNOWLEDGMENTS

The authors would like to thank Jim Frye, Tony Villanueva and Bill Resh of Chrysler Corporation for their support of this research. The authors would also like to thank Ed Probst and his staff at Delco Products for their assistance in supplying and testing hydraulic engine mounts.

REFERENCES

1. W. Resh 1994 Chrysler Corporation. Personal communication.
2. M. Bernuchon 1984 *SAE Paper* 840259. A new generation of engine mounts.
3. S. Bouchillon, R. Shoureshi, T. Knurek and P. Schlike 1989 *SAE Paper* 891160. Optimal tuning of adaptive hydraulic engine mounts.
4. R. M. Brach and A. G. Haddrow 1993 *SAE Paper* 931321. On the dynamic response of hydraulic engine mounts.
5. M. Clark 1985 *SAE Paper* 851650. Hydraulic engine mount isolation.
6. P. E. Corcoran and G.-H. Ticks 1984 *SAE Paper* 840407. Hydraulic engine mount characteristics.

7. W. C. Flower 1985 *SAE Paper* 850975. Understanding hydraulic mounts for improved vehicle noise, vibration and ride qualities.
8. K. Kadomatsu 1989 *SAE Paper* 891138. Hydraulic engine mount for shock isolation at acceleration on the FWD cars.
9. R. A. Muzechuk 1984 *SAE Paper* 840410. Hydraulic mounts—improved engine isolation.
10. R. Shoureshi, P. L. Graf and T. L. Houston 1986 *SAE Paper* 860549. Adaptive hydraulic engine mounts.
11. R. Singh, G. Kim and P. V. Ravindra 1992 *Journal of Sound and Vibration* **158**, 219–243. Linear analysis of automotive hydro-mechanical mount with emphasis on decoupler characteristics.
12. M. Sugino and E. Abe 1986 *SAE Paper* 861412. Optimum application for hydroelastic engine mount.
13. T. Ushijima and T. Dan 1986 *SAE Paper* 860550. Nonlinear B.B.A. for predicting vibration of vehicle with hydraulic engine mount.
14. T. Ushijima, K. Takano and H. Kojima 1988 *SAE Paper* 880073. High performance hydraulic mount for improving vehicle noise and vibration.
15. J. P. West 1987 *Automotive Engineer* **12**, 17–19. Hydraulically-damped engine mounts.
16. P. L. Graf, D. Novotny, R. Shoureshi, J. Starkey and R. W. Stevens 1988 *SAE Paper* 880074. Active frame vibration control for automotive vehicles with hydraulic engine mount.
17. G. Kim and R. Singh 1993 in *Advanced Automotive Technologies* (M. Ahmadian, editor). 247–255. New York: ASME. A broadband adaptive hydraulic mount system.
18. R. Shoureshi, P. L. Graf, S. Bouchillon, T. Knurek and R. W. Stevens 1988 *SAE Paper* 880075. Open-loop versus closed-loop control for hydraulic engine mounts.
19. G. Kim and R. Singh 1992 in *Transportation Systems*—1992, 165–180. New York, ASME. Resonance, isolation and shock control characteristics of automotive nonlinear hydraulic engine mounts.
20. G. Kim and R. Singh 1993 *Journal of Dynamic Systems, Measurement and Control* **115**, 482–487. Nonlinear analysis of automotive hydraulic engine mount.
21. C. T. Chang 1992 *Master's Thesis, Northwestern University*. Dynamic analysis of hydraulic engine mounts.
22. J. S. Bendat and A. G. Piersol 1986 *Random Data: Analysis and Measurement Procedures*. New York: John Wiley.
23. D. Karnopp and R. Rosenberg 1975 *System Dynamics: A Unified Approach*. New York: John Wiley.
24. H. M. Paynter 1961 *Analysis and Design of Engineering Systems*. Cambridge, Massachusetts: MIT Press.
25. Y. C. Chiou 1993 *Master's Thesis, Northwestern University*. Computer simulation of hydroelastic engine mounts.
26. G. F. Franklin, J. D. Powell and M. L. Workman 1990 *Digital Control of Dynamic Systems*. Reading, Massachusetts: Addison-Wesley.
27. S. Dubowsky and F. Freudenstein 1971 *Transactions of the American Society of Mechanical Engineers, Journal of Engineering for Industry* **93**, 310–316. Dynamic analysis of mechanical systems with clearances, Part 2: dynamic response.
28. R. J. Comparin and R. Singh 1989 *Journal of Sound and Vibration* **134**, 259–290. Non-linear frequency response characteristics of an impact pair.
29. D. F. Hays 1963 *Journal of Basic Engineering* **85**, 243–246. Squeeze films for rectangular plates.
30. W. S. Griffin, H. H. Richardson and S. Yamanami 1966 *Journal of Basic Engineering* **88**, 451–456. A study of fluid squeeze-film damping.
31. J. E. Gibson 1963 *Nonlinear Automatic Control*. New York: McGraw-Hill.
32. P.-T. D. Spanos and W. D. Iwan 1978 *International Journal of Non-linear Mechanics* **13**, 71–78. On the existence and uniqueness of solutions generated by equivalent linearization.
33. A. Gelb and W. Vander-Velde 1968 *Multiple-input Describing Functions and Nonlinear Systems Design*. New York: McGraw-Hill.
34. A. Ushida and L. O. Chua 1984 *IEEE Transactions on Circuits and Systems* **CAS-31**(9), 766–778. Frequency-domain analysis of nonlinear circuits driven by multi-tone signals.

APPENDIX A: ORIFICE PROPERTIES

A method of estimating orifice inertia, I_0, and damping, B_0, based on resonant frequency, ω_{r2}, and slope of the elastic rate plot at resonance, m_{r2}, is presented. The starting

point is equation (14), which provides an approximate expression for dynamic stiffness. It is convenient to define a natural frequency and damping ratio as

$$\omega_n = \sqrt{K_b/I_0}, \qquad \zeta = B_0/2\sqrt{K_b I_0}. \tag{A1}$$

The frequency response may then be written in terms of real (elastic rate) and imaginary (damping) parts,

$$K_{dyn}(\mathrm{j}\omega) = \left[K_r + A_p^2 K_b \frac{\alpha\omega^4 + (4\zeta^2 - \alpha)\omega_n^2\omega^2}{(\omega^2 - \omega_n^2)^2 + 4\zeta^2\omega_n^2\omega^2} \right] + \mathrm{j}\omega\left[B_r + A_p^2 K_b 2\zeta\omega_n \frac{2\zeta\omega_n^2 - (1-\alpha)\omega^2}{(\omega^2 - \omega_n^2)^2 + 4\zeta^2\omega_n^2\omega^2} \right], \tag{A2}$$

where $\alpha = 1 - A_d/A_p$. An expression for ω_{r2} is found by maximizing the damping term in equation (A2) with respect to frequency:

$$\omega_{r2}^2 = \omega_n^2[1 - \sqrt{4(1-\alpha)\zeta^2 + \alpha^2}]/(1-\alpha). \tag{A3}$$

It is now helpful to define β as

$$\beta = [1 - \sqrt{4(1-\alpha)\zeta^2 + \alpha^2}]/(1-\alpha). \tag{A4}$$

An expression for m_{r2} is found by differentiating the elastic rate term in equation (A2) with respect to frequency, and evaluating at $\omega = \omega_{r1}$:

$$m_{r2} = \frac{2A_p^2 K_b}{\omega_{r2}} \times \left[\frac{(2\alpha\beta^2 + \beta(4\zeta^2 - \alpha))((1-\beta)^2 + 4\zeta^2\beta) - 2(\beta^2 - \beta(2\zeta^2 - 1))(\alpha\beta^2 + \beta(4\zeta^2 - \alpha))}{((1-\beta)^2 + 4\zeta^2\beta)^2} \right]. \tag{A5}$$

Equation (A5) may be solved for ζ using a Newton–Raphson technique; subsequently, equation (A3) may be solved for ω_n. Determination of I_0 and B_0 is then straightforward using equations (A1).